JPRS-UEQ-90-009
21 JUNE 1990

FOREIGN BROADCAST INFORMATION SERVICE

# JPRS Report

# Science & Technology

## USSR: Engineering & Equipment

JPRS-UEQ-90-009
21 JUNE 1990

# SCIENCE & TECHNOLOGY

# USSR: ENGINEERING & EQUIPMENT

## CONTENTS

INDUSTRIAL TECHNOLOGY, PLANNING, PRODUCTIVITY

UDC 531.55:531.2

# MINIMUM-FUEL OPTIMAL MULTIPULSE APSIDAL INTERORBITAL FLIGHTS

907F0286A Leningrad VESTNIK LENINGRADSKOGO UNIVERSITETA: MATEMATIKA, MEKHANIKA, ASTRONOMIYA in Russian No 1, Jan 90 (manuscript received 6 Apr 89) pp 63-67

[Article by S. N. Kirpichnikov]

[Text] The problem of finding minimum-fuel optimal pulsed flight trajectories between Keplerian orbits in a central Newtonian gravitational field is studied. The time of motion along the orbits is free. Unlike the similar problem of interorbital flight, in which the orbit of the flight from the initial to the final orbit must be constructed, one must construct a flight trajectory, begun on the initial orbit and which only intersects the final orbit, in the considered problem of interorbital flight, so that the equalizing pulse rate at the finish point is not achieved. The characteristic maneuvering speed is minimized with the following assumptions: 1) "fragmentation" of the pulses is not permitted, 2) the total number of pulses is $n \leq N$, where $N$ is given ($N = 1, 2, \ldots$), and 3) the flow rates of gases during all pulses are identical.

Let us first consider the case of coplanar boundary orbits. Using argument [1], it is easy to prove the following statement, which permits one to limit oneself to coplanar postulation of the problem.

Theorem 1. The trajectory of an minimum-fuel pulsed flight between coplanar boundary orbits lies in the plane of these orbits.

The author [2-4] studied the coplanar problem of finding minimum-fuel optimal single-pulse ($N = 1$) flight. Using the methods of these articles, it is easy to prove the following statements, somewhat more general compared to the indicated articles, about the type of steady and optimal orbits of pulsed flights in the coplanar problem.

Theorem 2. Any fixed orbit in the problem of an minimum-fuel optimal single-pulse flight always touches the final orbit at the finish point.

Corollary. A limited fixed multipulse orbit in the problem of an minimum-fuel optimal interorbital flight always touches the final orbit at the finish point.

The following four theorems are related to fixed and optimal single-pulse (N = 1) orbits in the coplanar problem of finding minimum-fuel optimal trajectories of interorbital flights.

Theorem 3. The radial pulse may not be fixed in any boundary orbits at all.

Theorem 4. The tangential pulse can be fixed only if the lines of the apsides of the boundary orbits coincide (specifically, if at least one of them is circular), and single-pulse flight is apsidal, i.e., both apsides of the Keplerian orbit of the flight coincide with the apsides of the boundary orbits.

Theorem 5. Let the boundary orbits have a common line of apsides or at least let one of them be circular. The apsidal maneuvers and only these maneuvers are fixed single-pulse maneuvers in the considered extreme problem.

Theorem 6. Let the difference of the angular distances of the pericenters of the boundary orbits be a multiple of $\pi$ or at least one of them is circular. If the final orbit is located entirely outside (inside) the initial orbit, the global optimal maneuver of a single-pulse flight is an apsidal maneuver, which ends at the pericenter (apocenter) of the final orbit.

A system of necessary conditions, derived in [2], is used in the proof of these theorems and the case of intersecting boundary orbits, trivial in the problem of an interorbital flight with free time, is eliminated from the consideration here and below. The following easily proved theorem guarantees the absence of abnormal solutions (gradients of the left sides of the coupling equations in the system of necessary conditions are linearly dependent) in the coplanar problem of an minimum-fuel optimal pulse flight between nonintersecting boundary orbits.

Theorem 7. Abnormal solutions are possible in any extreme problem of constructing interorbital single-pulse flights or two-pulse flights with free time only upon touching the boundary orbits. These solutions are characterized by touching all three orbits (the initial, intermediate and final at a common point--the point of the start and finish).

It was established above for coplanar boundary orbits with coincident apsidal lines that fixed and globally optimal single-pulse flights are apsidal. Let us study in this regard for the boundary orbits below the problem of the minimum-fuel optimality of apsidal multipulse interorbital flights.

Let us continue as before to assume that the problem is coplanar. It is easy to see that trajectories with apsidal tangential connections of all Keplerian branches and the maximum cases of these connections--apsidal tangential drifts to infinity and returns from infinity along parabolas--satisfy the system of necessary conditions in the case of boundary orbits with common line of apsides of the corresponding considered extreme problem. Let us also call the trajectories apsidal due to the brevity of them. The following statement determines the sufficient conditions of global optimality of apsidal trajectories.

Theorem 8. If the orientation of one of the boundary orbits is arbitrary in the coplanar problem of interorbital pulsed flight (for example, if at least one of them is circular), the characteristic maneuvering speed assumes the least value on the apsidal trajectories when the lines of the apsides of boundary orbits coincide. If the final orbit is located outside (inside) the initial orbit, the globally optimal maneuver with limited flight trajectory terminates at the pericenter (apocenter) of the final orbit, while the difference of the angular distances of the pericenters of the boundary orbits should be equal to $(2k + 1)\pi$, where k is an integer, for single-pulsed flight.

Common geometric properties of transversally [5] intersecting curves on a plane and also some results of [1, 6-8] and methods used there to study the problems of interorbital flights are used in proof of this and all subsequent theorems.

Thus, let the boundary orbits now be coplanar and have a common line of apsides. Let us study the apsidal trajectories with $N = 2$. Two new types are possible besides the above apsidal single-pulse trajectories. These are primarily bielliptic apsidal trajectories. The start is made at the apsida of the initial orbit (polar radius $r_1$) and the finish is made at the apsides of the final orbit (polar radius $r_2$), and both corresponding apsidal points lie on the same semiaxis of the common line of apsides of the boundary orbits. The additional (second) apsidal tangential pulse is made on the opposite semiaxis of this line at a point with the polar radius $\rho > 0$. Finally, both semiellipses of the bielliptical apsidal trajectory change to parabolas in the final case at $\rho = \infty$, and the additional pulse becomes "zero" at infinity. The flight and its trajectory in this limiting case is called biparabolic. We note that the trajectory of biparabolic flight with such a small increase of the characteristic velocity can be approximated in practice by a bielliptical apsidal trajectory with rather large $\rho$.

Theorem 9. Let the boundary orbits have a common line of apsides. Only single-pulse and biparabolic flights can be optimal in the class of flights with single- and two-pulse trajectories ($N = 2$). It is necessary that $r_1 \geq 4r_2$ for optimality of a biparabolic flight.

Let us formulate the auxiliary obvious statement in the form of a lemma.

Lemma. A pulse drift maneuver, minimal according to the characteristic speed, with given initial Keplerian orbit to infinity is always single-pulse, and the pulse is tangential and is made at the pericenter of the initial orbit.

Let us now remove the constraint N = 2. The following theorem is easily proved by the method of mathematical induction with regard to theorem 9 and the lemma.

Theorem 10. Let the boundary orbits have a common line of apsides. Further, let the apsides of the initial and final orbits, lying on the same semiaxis OL of this line, have polar radii $r_1$ and $r_2$, respectively. If $\max(r_1/r_2) < 4$ upon two possible selections of semiaxis OL, some single-pulse flight is globally optimal in the class of minimum-fuel optimal flights with pulsed apsidal trajectories, and either biparabolic flight with start at the pericenter of the initial orbit or a single-pulse flight is globally optimal in the opposite case. Specifically, if the initial orbit is located inside the final orbit or if $r_{1A} < 4r_{2\Pi}$ ($r_{1A}$ is the distance of the apocenter of the initial orbit and $r_{2\Pi}$ is the distance of the pericenter of the final orbit), only single-pulse flights can be globally optimal.

Let us now take the assumption of the coplanarity of the problem.

Theorem 11. If the biparabolic flight is globally optimal in the coplanar problem of a minimum-fuel optimal pulse interorbital flight with arbitrary orientation of one of the boundary orbits, biparabolic flight in the plane of the initial orbit will also be globally optimal in any problem of minimum-fuel optimal pulsed flight with arbitrarily given arrangement of boundary orbits in space of the same dimensions and shape.

The statements of theorems 10 and 11 permit considerable amplification for the case of circular boundary orbits.

Theorem 12. A Hohmann single-pulse flight (see [2]) is globally optimal in the class of minimum-fuel pulsed optimal flights between circular both coplanar and noncoplanar boundary orbits of radii $r_1$ and $r_2$, if $r_1/r_2 \leq 4.828\ldots$, and biparabolic flight is globally optimal if $r_1/r_2 \geq 4.828\ldots$. Any two-pulse apsidal bielliptic orbit with $\rho > r_1$ is more optimal than a Hohmann single-pulse flight for $r_1/r_2 > 5.879\ldots$. Finally, there is a critical value $\rho_* > r_1$ for any $r_1$, $r_2$, $r_1/r_2 \in (4.828\ldots, 5.879\ldots)$, beginning with which a bielliptical apsidal two-pulse flight is more optimal than a Hohmann single-pulse flight for any $\rho > \rho_*$, and the economy of the characteristic speed is greater, the greater $\rho$, $\rho > \rho_*$. All the considered maneuvers are made in the plane of the initial orbit.

Comment. The precise value of constant 4.828... is equal to $(\sqrt{2} - 1)^{-2} - 1$. Constant 5.879... is the greatest real root of the equation

$$x^4 - 9x^3 + 15x^2 + 19x + 4 = 0.$$

We note in conclusion that constants 4.828... and 5.879... under conditions of theorem 12 play the same role as constants 11.938... and 15.581... in the theory of minimum-fuel optimal pulsed interorbital flights (see, for example, [9], section 3.2), but, unlike the latter, the conditions of theorem 12 are considerably nonsymmetrical in the considered theory with respect to radii $r_1$ and $r_2$ of the initial and final orbits.

BIBLIOGRAPHY


1. Ting, Lu, ARS JOURNAL, Vol 30, No 11, 1960.

2. Kirpichnikov, S. N., VESTNIK LENINGRADSKOGO UNIVERSITETA, No 1, 1964.

3. Kirpichnikov, S. N., VESTNIK LENINGRADSKOGO UNIVERSITETA, No 7, 1964.

4. Kirpichnikov, S. N., BYULLETEN INSTITUTA TEORETICHESKOY ASTRONOMII AKADEMII NAUK SSSR, Vol 10, No 10 (123), 1966.

5. Poston, T. and I. Stewart, "Teoriya katastrof i yeye prilozheniya" [Catastrophy Theory and Its Applications], Moscow, 1980.

6. Louden, D. F., "Metody optimizatsii s prilozheniyami k mekhanike kosmicheskogo poleta" [Methods of Optimization With Applications to the Mechanics of Space Flight], edited by J. Leitman, Moscow, 1965.

7. Ting Lu, ASTRONAUTICA ACTA, Vol 6, No 5, 1960.

8. Ivashkin, V. V., "Optimizatsiya kosmicheskikh manevrov" [Optimization of Space Maneuvers], Moscow, 1975.

9. Escobal, P., "Metody astrodinamiki" [Methods of Astrodynamics], Moscow, 1971.

UDC 531.36:521.1

# ON ONE FORM OF DIFFERENTIAL EQUATIONS OF PERTURBED MOTION OF GRAVITY-ORIENTED SOLID

907F0286B Leningrad VESTNIK LENINGRADSKOGO UNIVERSITETA: MATEMATIKA, MEKHANIKA, ASTRONOMIYA in Russian No 1, Jan 90 (manuscript received 8 Jun 89) pp 71-75

[Article by A. A. Tikhonov]

[Text] Difficulties frequently arise in construction of the transformed system of differential equations of motion when solving nonlinear problems of mechanics using approximate analytical methods, which provide transition to new variables. These difficulties can sometimes be overcome to a significant degree by using the method of variation of canonical random constants.

This method is a convenient means of constructing differential equations of the perturbed motion of mechanical systems, the state of which can be described by canonical equations. Thus, the method of variation of canonical random constants in combination with averaging the differential equations was used successfully in [1, 2] to study quasi-linear vibrations of a solid exposed to gravitational forces in the neighborhood of the position of stable equilibrium.

A form of notation of differential equations of perturbed motion of a gravity-oriented solid, convenient for study and which generalizes the corresponding equations used in [1, 2] for the case of potential perturbing forces, is found in this paper. The rotational moment of the solid with respect to its center of mass, moving in a circular Keplerian orbit in a central gravitational field, is studied on the assumption that nonpotential forces that allow quadratic approximation are acting on the body in a central gravitational field.

Two coordinate systems with common origin at the center of mass of the body are introduced into consideration: $c\xi\eta\zeta$--an orbital coordinate system (OSK) (axis $\zeta$ is directed along the radius vector of the center of mass of the body with respect to the attracting center, axis $\xi$ is directed along the tangent to the orbit in the direction of motion, and axis $\eta$ is directed along the normal to the orbital plane, $cxyz$ is rigidly bound to the body so that its axes are directed along the main

central axis of inertia of the body, $\xi_0$, $\eta_0$, $\zeta_0$ and i, j, k are the unit vectors of axes $\xi$, $\eta$, and $\zeta$ and x, y, z, respectively, which satisfy the equalities $\xi_0 = \alpha_1 \mathbf{i} + \alpha_2 \mathbf{j} + \alpha_3 \mathbf{k}$, $\eta_0 = \beta_1 \mathbf{i} + \beta_2 \mathbf{j} + \beta_3 \mathbf{k}$, $\zeta_0 = \gamma_1 \mathbf{i} + \gamma_2 \mathbf{j} + \gamma_3 \mathbf{k}$, . where $\alpha_i$, $\beta_i$, $\gamma_i$ $(i = \overline{1, 3})$ are direction cosines.

The following notations are adopted in the paper: $\omega = \omega_0 + \omega'$ is the absolute angular velocity of the body, $\omega_0 = \omega_0 \eta_0$ is the angular velocity of the OSK, $\omega' = pi + qj + rk$ is the angular velocity of the body with respect to the OSK, and A, B, and C are the principal central moments of inertia of the body.

Differential Euler equations of rotational motion of the body due to the effect of gravitational moment $M_\Gamma$ and of a general perturbing nonpotential moment $\mathbf{M}_B (|\mathbf{M}_B| \ll |\mathbf{M}_\Gamma|)$ have the form

$$\frac{d}{dt}(\Lambda\omega) + \omega \times (\Lambda\omega) = \mathbf{M}_\Gamma + \mathbf{M}_B, \tag{1}$$

where $\Lambda = \mathrm{diag}\ (A, B, C)$, $\mathbf{M}_\Gamma = 3\omega_0^2 \zeta_0 \times (\Lambda\zeta_0)$, $\mathbf{M}_B$ is the analytical vector function of variables $\alpha_i$, $\beta_i$, $\gamma_i$, $p$, $q$, $r$ $(i = \overline{1, 3})$, generally non-autonomous. Equation (1) together with kinematic Poisson equations

$$\frac{d\xi_0}{dt} = \xi_0 \times \omega - \omega_0 \zeta_0, \quad \frac{d\eta_0}{dt} = \eta_0 \times \omega, \quad \frac{d\zeta_0}{dt} = \zeta_0 \times \omega + \omega_0 \xi_0 \tag{2}$$

form a closed differential system.

If there are no perturbing moment and fulfillment of the conditions of gravitational orientation B > A > C [2], the body has a stable position of equilibrium $\alpha_1 = \beta_2 = \gamma_3 = 1$ in the OSK, taken as unperturbed motion. It is determined by equalities $\psi = \varphi = \theta = 0$ in "aircraft" angles of orientation (see figure).

Posing the problem of finding a system of differential equations of perturbed motion in a form convenient for study of quasi-linear vibrations of a gravity-oriented solid, let us consider the nonlinear component of the gravitational moment as perturbation along with perturbing moment $M_B$.

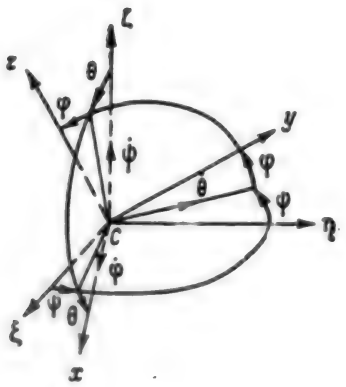


Following [1, 2], let us construct a perturbed differential system using canonical variables. Let us introduce the following canonical variables: $\psi$, $\varphi$, $\theta$, $p_1$, $p_2$ $p_3$, where $p_1 = \frac{\partial L}{\partial \dot{\psi}} = -A\omega_x \sin\theta + B\omega_y \sin\varphi\cos\theta + C\omega_z \cos\varphi\cos\theta$, $p_2 = \frac{\partial L}{\partial \dot{\varphi}} = A\omega_x$, $p_3 = \frac{\partial L}{\partial \dot{\theta}} + B\omega_0 = B\omega_y \cos\varphi - C\omega_z \sin\varphi + B\omega_0$; $L = \frac{1}{2}(A\omega_x^2 + B\omega_y^2 + C\omega_z^2) - \frac{3}{2}\omega_0^2[(A-C)\gamma_1^2 + (B-C)\gamma_2^2]$ is a Lagrange function, in which $\omega_x$, $\omega_y$, $\omega_z$, $\gamma_1$, and $\gamma_2$ are expressed by $\psi$, $\varphi$, $\theta$, $\dot{\psi}$, $\dot{\varphi}$, $\dot{\theta}$ on the basis of kinematic formulas: $p = \dot{\varphi} - \dot{\psi}\sin\theta$, $q = \dot{\theta}\cos\varphi + \dot{\psi}\sin\varphi\cos\theta$, $r = \dot{\psi}\cos\varphi\cos\theta - \dot{\theta}\sin\varphi$, $\gamma_1 = -\sin\theta$, $\gamma_2 = \sin\varphi\cos\theta$. For the projections of relative angular velocity $\omega'$, we will have

$$p = A^{-1}p_2 - \omega_0 \sin\psi\cos\theta,\ q = B^{-1}[(p_3 + B\omega_0)\cos\varphi + (p_1 + p_2\sin\theta)\times \sin\varphi\cos^{-1}\theta] - \omega_0(\sin\psi\sin\varphi\sin\theta + \cos\psi\cos\varphi),\ r = C^{-1}[-(p_3 + B\omega_0)\times \sin\varphi + (p_1 + p_2\sin\theta)\cos\varphi\cos^{-1}\theta] - \omega_0(\sin\psi\cos\varphi\sin\theta - \cos\psi\sin\varphi). \quad (3)$$

Turning to the new independent variable $u = \omega_0 t$, let us introduce the dimensionless variables

$$\tilde{\psi}' = (C\omega_0)^{-1}p_1 + (1 - BC^{-1})\varphi,\ \tilde{\varphi}' = (A\omega_0)^{-1}p_2 - \psi,\ \tilde{\theta}' = (B\omega_0)^{-1}p_3. \quad (4)$$

Formulas (4), which coincide with linearized expressions (3), divided by $\omega_0$, are taken as the transition formulas from generalized pulses $p_i$ to new variables $\tilde{\psi}'$, $\tilde{\varphi}'$, $\tilde{\theta}'$ of the same order of smallness. Expressing

$\omega_x, \omega_y, \omega_z, \alpha_i, \beta_i, \gamma_i$ $(i=\overline{1,3})$ by $\tilde{\psi}', \tilde{\varphi}', \tilde{\theta}'$ and retaining terms no higher than second order of smallness with respect to the introduced dimensionless variables, let us transform system (1) and (2) to the form

$$\begin{aligned}&(\varphi')'=F_1,\ \psi'=\tilde{\psi}'+\varepsilon^{-1}\tilde{\varphi}'\theta+(1-\delta\varepsilon^{-1})\,\tilde{\theta}'\varphi+(\varepsilon^{-1}-1)\,\psi\theta,\\&\varepsilon\delta^{-1}\varphi\,(\tilde{\psi}')'+(\tilde{\theta}')'=F_2,\ \varphi'=\tilde{\varphi}'+\tilde{\psi}'\theta,\\&(\tilde{\psi}')'+\varepsilon^{-1}\theta\,(\tilde{\varphi}')'-\delta\varepsilon^{-1}\varphi\,(\tilde{\theta}')'=F_3,\ \theta'=\tilde{\theta}'+(\varepsilon\delta^{-1}-1)\,(\tilde{\psi}'\varphi-\varphi^2)+\frac{1}{2}\,\psi^2,\end{aligned}\qquad(5)$$

where $F_1=\varepsilon^{-1}[4\varepsilon(\varepsilon-\delta)\varphi-\varepsilon(1-\delta+\varepsilon)\tilde{\psi}'+(\varepsilon-\delta)((\delta+\varepsilon-1)\varphi\tilde{\theta}'-\varepsilon\tilde{\psi}'\tilde{\theta}')-$
$-(1-\delta+\varepsilon)\theta\tilde{\varphi}'+(\delta-1)\psi\theta]+\tilde{M}_x,\ F_2=\delta^{-1}[3(\varepsilon-1)\theta-\tilde{\psi}'\tilde{\varphi}'+(1-\delta+\varepsilon)\varphi\tilde{\varphi}'+$
$+(1-\varepsilon)(\psi\varphi-\psi\tilde{\psi}')]+\tilde{M}_y,\ F_3=\varepsilon^{-1}[(1-\delta+\varepsilon)\tilde{\varphi}'-(\delta-1)(\psi+3\varphi\theta)+$
$+(\varepsilon-1)\theta\tilde{\psi}'-\delta\psi\tilde{\theta}']+\tilde{M}_z,\ \tilde{M}_x=(A\omega_0^2)^{-1}M_{bx},\ \tilde{M}_y=(\delta A\omega_0^2)^{-1}M_{by},\ M_z=$
$=(\varepsilon A\omega_0^2)^{-1}M_{bz}$ are expressions, calculated with regard to quadratic terms and $\delta=BA^{-1},\ \varepsilon=CA^{-1}$.

System (5) at $M_B = 0$ permits a canonical form of notation with Hamiltonian $H = H_0 + H_1$, where $H_0=\frac{1}{2}(A\tilde{\varphi}'^2+B\tilde{\theta}'^2+C\tilde{\psi}'^2)+\frac{1}{2}[4(B-C)\varphi^2+$ $+\ 3(A-C)\theta^2+(B-A)\psi^2]$ and $H_1=\frac{1}{2}[2(C-B)(\tilde{\psi}'-\varphi)\tilde{\theta}'\varphi+2(A-C)\tilde{\psi}'\psi\theta+$ $+\ 2A\tilde{\psi}'\tilde{\varphi}'\theta+B\tilde{\theta}'\psi^2]+(C-B)\psi\varphi\theta$ are components of second and third orders of smallness, respectively. Linear approximation of this system, corresponding to Hamiltonian $H_0$, i.e., an unperturbed differential system, has a general solution of type

$$\psi=\sum_{i=1}^{2}\sigma_{1i}\sqrt{x_i}\sin\tau_i,\ \varphi=\sum_{i=1}^{2}\sigma_{2i}\sqrt{x_i}\cos\tau_i,\ \theta=\sqrt{2B^{-1}x_3}\,k_3^{-1}\sin\tau_3,\qquad(6)$$

$$\tilde{\psi}'=\sum_{i=1}^{2}k_i\sigma_{1i}\sqrt{x_i}\cos\tau_i,\ \tilde{\varphi}'=-\sum_{i=1}^{2}k_i\sigma_{2i}\sqrt{x_i}\sin\tau_i,\ \tilde{\theta}'=\sqrt{2B^{-1}x_3}\cos\tau_3,\qquad(7)$$

where $\tau_j=k_j(u+v_j)$ $(j=\overline{1,3})$; $x_i, v_j$ $(j=\overline{1,3})$ are canonical arbitrary constants and $k_j$ $(j=\overline{1,3})$ are unperturbed natural frequencies of the body:

$$k_{1,2}=\sqrt{a/2\mp\sqrt{a^2/4-b}},\ k_3=\sqrt{3(1-\varepsilon)\delta^{-1}},\ a=1+3(\delta-\varepsilon)+b/4,$$
$$b=4\varepsilon^{-1}(\delta-1)(\delta-\varepsilon);\ \sigma_{1i}=\sqrt{2}\,\varkappa_i k_i^{-1}\sqrt{A_i^{-1}},\ \sigma_{2i}=-\sqrt{2}\,k_i^{-1}\sqrt{A_i^{-1}},$$
$$A_i=\frac{(-1)^i B\varepsilon\left(k_1^2-k_2^2\right)}{\delta\left(\delta-1-\varepsilon k_i^2\right)},\ \varkappa_i=\frac{k_i(1-\delta+\varepsilon)}{\delta-1-\varepsilon k_i^2}\ (i=1,\ 2).$$

The inequalities $A_i>0$ $(i=1, 2)$, $\varkappa_1>0$, $\varkappa_2<0$, $\sigma_{11}>0$, $\sigma_{12}<0$, $\sigma_{21}<0$, $\sigma_{22}<0$. are valid in the region B > A > C.

Solution of system (5) by the method of variation of arbitrary constants $x_i$, $v_i$ $(i=\overline{1,3})$ is sought in the form of (6), where $x_i$ and $v_i$ are new unknown functions subject to determination.

Observation. It follows from the kinematic equations of system (5), written in variables $x_i$ and $v_i$, that the values of $x'_i$ and $v'_i$ have the order $O(\sqrt{x^3_i})$ and $O(\sqrt{x_i})$, respectively. Taking these estimates into account and also taking into account that the differential equations of perturbed motion with respect to conditions of postulation of the problem should contain terms no higher than second order of smallness with respect to $\psi$, $\varphi$, $\theta$, $\tilde{\psi}'$, $\tilde{\varphi}'$, $\tilde{\theta}'$ in derivatives $(\tilde{\psi}')'\varphi$, $(\tilde{\varphi}')'\theta$, $(\tilde{\theta}')'\varphi$, contained on the left sides of the dynamic equations of system (5), and one should accordingly leave only the following terms of second order of smallness: $\varphi\sum_{i=1}^{2}k_i^2\times\ \sigma_{1i}\sqrt{x_i}\sin\tau_i;\ -\theta\sum_{i=1}^{2}k_i^2\sigma_{2i}\sqrt{x_i}\cos\tau_i;\ -\varphi k_3\sqrt{2B^{-1}x_3}\sin\tau_3$,

where $\varphi$ and $\theta$ are determined by formulas (6).

Turning in system (5) to variables $x_i$ and $v_i$ according to transform (6) and (7) and solving it with respect to the derivatives, we find the desired system of differential equations of perturbed motion of the body, which can be written in the form

$$x'_i=-\frac{\partial H_1}{\partial v_i}+2(-1)^i\sqrt{x_i}\left[\sigma_{1,3-i}\sigma_1^{-1}\widetilde{M}_x\sin\tau_i-\sigma_{2,3-i}\sigma_2^{-1}\widetilde{M}_z\cos\tau_i\right],$$
$$v'_i=\frac{\partial H_1}{\partial x_i}+\left(k_i\sqrt{x_i}\right)^{-1}(-1)^i\left[\sigma_{1,3-i}\sigma_1^{-1}\widetilde{M}_z\cos\tau_i-\sigma_{2,3-i}\sigma_2^{-1}\widetilde{M}_z\sin\tau_i\right],$$
$$x'_3=-\frac{\partial H_1}{\partial v_3}+\sqrt{2Bx_3}\widetilde{M}_y\cos\tau_3,\ v'_3=\frac{\partial H_1}{\partial x_3}-\frac{\sqrt{B}}{k_3\sqrt{2x_3}}\widetilde{M}_y\sin\tau_3.$$

Here $i=1, 2$; $\sigma_1=k_1\sigma_{12}\sigma_{21}-k_2\sigma_{11}\sigma_{22}$, $\sigma_2=k_1\sigma_{11}\sigma_{22}-k_2\sigma_{12}\sigma_{21}$, and the expression for $H_1$ in variables $x_i$, $v_i$ has the form

$$H_1 = (h_1x_1 + h_2x_2)\sqrt{x_3}\cos\tau_3 + h_3x_1\sqrt{x_3}\cos(2\tau_1+\tau_3) + h_4x_1\sqrt{x_3}\times$$
$$\times\cos(2\tau_1-\tau_3) + h_5x_2\sqrt{x_3}\cos(2\tau_2+\tau_3) + h_6x_2\sqrt{x_3}\cos(2\tau_2-\tau_3) +$$
$$+ h_7\sqrt{x_1x_2x_3}\cos(\tau_1+\tau_3-\tau_2) + h_8\sqrt{x_1x_2x_3}\cos(\tau_2+\tau_3-\tau_1) +$$
$$+ h_9\sqrt{x_1x_2x_3}\cos(\tau_1+\tau_2-\tau_3) + h_{10}\sqrt{x_1x_2x_3}\cos(\tau_1+\tau_2+\tau_3),$$

where $h_\alpha = \sqrt{B/2}\left[(\varepsilon\delta^{-1}-1)(k_\alpha\sigma_{1\alpha}-\sigma_{2\alpha})\sigma_{2\alpha} + \sigma_{1\alpha}^2/2\right]$ $(\alpha=1,\ 2)$,

$$h_\beta = \sqrt{B/8}\left[(\varepsilon\delta^{-1}-1)\sigma_{2i}(k_i\sigma_{1i}-\sigma_{2i}+(-1)^\beta k_3^{-1}\sigma_{1i}) - \sigma_{1i}^2/2+(-1)^\beta\delta^{-1}k_i\times\right.$$
$$\left.\times k_3^{-1}\sigma_{1i}[(1-\varepsilon)\sigma_{1i}-k_i\sigma_{2i}]\right]$$ $(i=1$ для $\beta=3,\ 4;\ i=2$ for $\beta=5,\ 6)$,

$$h_\gamma = \sqrt{B/8}\left[(\varepsilon\delta^{-1}-1)\sigma_3 - (-1)^\gamma k_3^{-1}\delta^{-1}\sum_{i=1}^{2}(-1)^i k_{3-i}\sigma_{1,3-i}[(1-\varepsilon)\sigma_{1i}-k_i\sigma_{2i}]+\right.$$
$$\left.+(-1)^\gamma k_3^{-1}(1-\varepsilon)(\sigma_{12}\sigma_{21}-\sigma_{11}\sigma_{22})+\sigma_{11}\sigma_{12}\right]$$ $(\gamma=7,\ 8)$,

$$h_\nu = \sqrt{B/8}\left[(\varepsilon\delta^{-1}-1)\sigma_3 + (-1)^\nu k_3^{-1}\delta^{-1}[(k_1k_2+\delta-\varepsilon)(\sigma_{11}\sigma_{22}+\sigma_{12}\sigma_{21})-\right.$$
$$\left.-(1-\varepsilon)(k_1+k_2)\sigma_{11}\sigma_{12}] - \sigma_{11}\sigma_{12}\right]$$ $(\nu=9,\ 10)$,

$$\sigma_3 = k_1\sigma_{11}\sigma_{22} + k_2\sigma_{12}\sigma_{21} - 2\sigma_{21}\sigma_{22}.$$

The convenience of using the derived differential equations of perturbed motion in the form of (8) for study of quasi-linear vibrations of a solid is determined by the following circumstances: 1) the structure of these equations is such that their right sides are divided into two groups of terms, from which the first, written in canonical form, corresponds to "canonical" perturbations, caused in the given case of nonlinear quadratic terms at the gravitational moment, while the second group corresponds to "noncanonical" perturbations due to moment $M_B$, generally being of an arbitrary nature; and 2) system (8) has a form that permits direct use without laborious computations of asymptotic methods of nonlinear mechanics for study of it.

Equations (8) are canonical in the absence of a perturbing moment $M_B$ and coincide with the widely used equations in canonical variations [2].

## BIBLIOGRAPHY


1. Breakwell, J. V. and R. Pringle, Jr., "Proceedings of the 16th International Astronautical Congress, Vol 6, Athens, 1965, 1966.

2. Beletskiy, V. V., "Dvizheniye sputnika otnositelno tsentra mass v gravitatsionnom pole" [The Motion of a Satellite With Respect to the Center of Mass in a Gravitational Field], Moscow, 1975.

UDC [621.311.25:621.039]:620.193.4.091.45

**Some Features of Corrosion Processes in Chemical Cleaning of AES Heat Exchanger Equipment**

907F0210A Moscow ELEKTRICHESKIYE STANTSII in Russian, No 2 Feb 90, pp 13-16

[Article by N.N. Berezkin, engineer, Yuzhtekhenergo; and S.S. Kirilyuk, C.Chem.S., Lvov State Medical Institute]

[Text] An aqueous solution of a synthetic low-molecular organic acid (NMK) is often used as a cleaning agent during the process of chemical cleaning of carbonaceous deposits on heat exchanger equipment. Use of this acid in AESs involves the particular characteristics of the structural materials in the primary equipment[1,2]. As was shown in [3,4], steps need to be taken to reduce the rate of corrosion of the equipment during cleaning in connection with the aggressiveness of the cleaning solution as compared to the metal from which the deposits are being removed.

One method of reducing corrosion in the copper alloys used as the primary material in the manufacture of heat exchangers is the protective screen method. Before chemical cleaning, protectors – steel plates – are mounted along the loop being washed. According to the data in the literature one may say that the rate of corrosion of the protectors increases sharply, taking most of the load of the corrosion process upon themselves, and because of this the rate of corrosion in the primary material of the heat exchanger, in particular MNZh-5-1, should be reduced considerably; MNZh-5-1 is used mainly in the manufacture of the tubing systems for the condensers in turbines for high power generating units.

However, we should note that as the steel protectors dissolve, an additional significant amount of trivalent iron ions land on the loop being cleaned, and the effect on the nature of the corrosion process is clear: there is a dramatic increase in copper alloy corrosion, i.e. intense wear of the heat exchanger during chemical cleaning. Even if protective screening is not used, steel structures along the loop – condenser tube plates, tubing intakes and drain pipes – may take the place of the protectors.

As experience has shown in the use of periodic chemical cleaning, a lot of cleaning solution (and, hence, money) is lost at the ends of condenser intakes and drain pipes and in the places where the tubes roll around in the tube plates, i.e. where intense local corrosional wear takes place.

With the idea of reducing the impact of trivalent iron ions on the corrosion rate of copper alloys in acidic cleaning solutions, we recommend the introduction of compounds that facilitate the transfer of trivalent iron to the divalent state [3]. Thiourea is widely employed for this purpose, in addition to a number of other compounds. However, the corrosion process in which steel and MNZh-5-1 alloy are present together in acidic solutions with admixed reducing compounds inhibitory to acidic corrosion has not been studied enough. There is cause for interest in carrying out an investigation in this area.

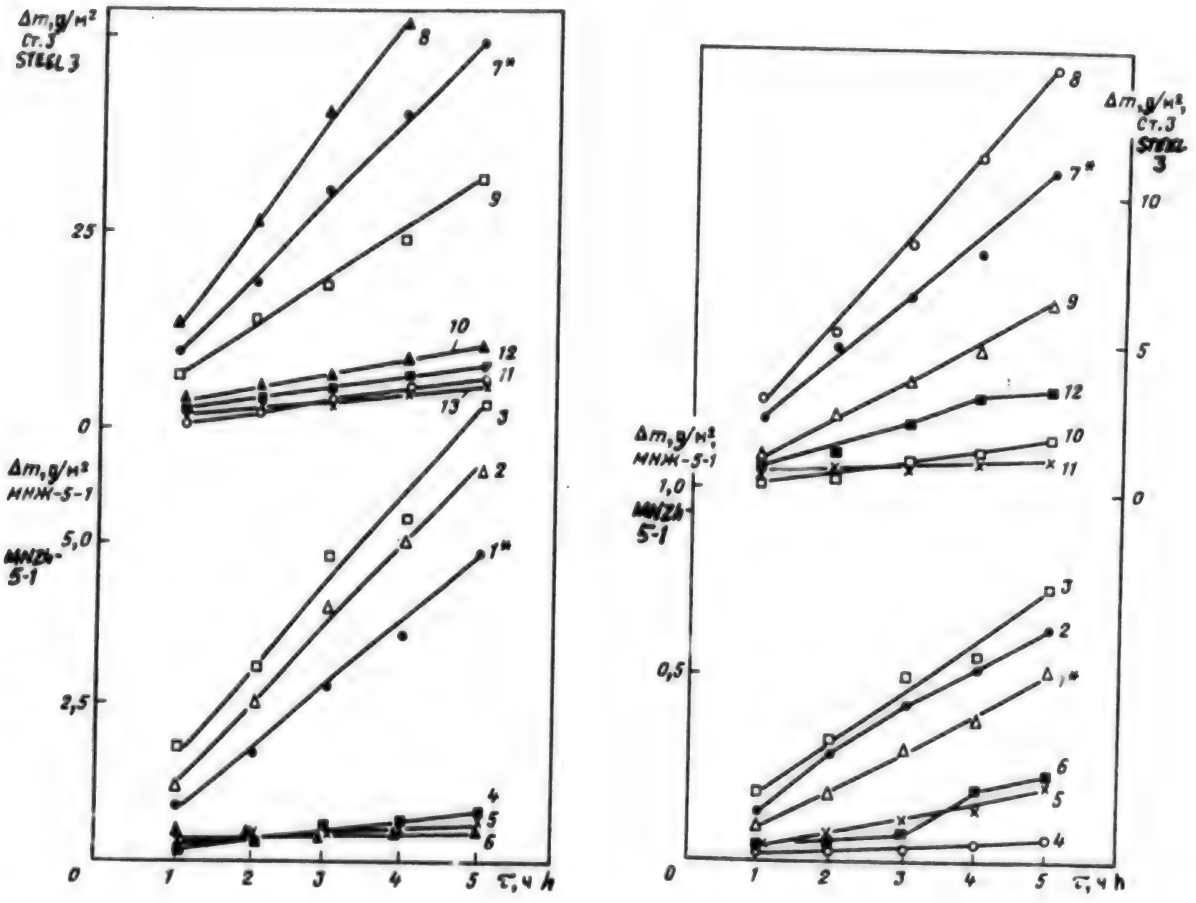


**Figure 1. A Graph of the Corrosion Processes For MNZh-5-1 and Steel 3 Being Present Together in a 7% NMK Solution, $T = 333$ K:** *1* – MNZh-5-1 corrosion rate (No Steel 3 present); *2* – MNZh-5-1 corrosion rate; *3* – effect of thiourea (0.25 g/dm$^3$) on the MNZh-5-1 corrosion rate; *4 – 6* – protective action of acidic corrosion inhibitors (US-1, R-12, R-14, R-15) on MNZh-5-1; *7* – Steel 3 corrosion rate (no MNZh-5-1 present); *8* – Steel 3 corrosion rate; *9* – effect of thiourea (0.25 g/dm$^3$) on the Steel 3 corrosion rate; *10 – 13* – protective action of acidic corrosion inhibitors (US-1, R-12, R-14, R-15) on Steel 3

**Figure 2. A Graph of the Corrosion Processes for MNZh-5-1 and Steel 3 Being Present Together in a 7% NMK Solution, $T = 313$ K:** Notation the same as for Figure 1.

The methodology for conducting a laboratory experiment has already been described [1,2]. Steel 3 and MNZh-5-1 samples are simultaneously placed in chemical beakers containing a 7% NMK solution, to which thiourea is added (0.25, 0.5 and 1.0 g/dm$^3$, tests 3 – 5, see Table), as well as certain acidic corrosion inhibitors that we synthesized ourselves (US-1, R-12, R-14, R-15), having a constant concentration of 0.5 g/dm$^3$ (tests 6 – 9, see Table). In addition, Steel 3 and MNZh-1-5 were placed in beakers with NMK separately (test 1) and together (test 2) without adding thiourea or inhibitor in order to study the effect of MNZh-5-1 on the corrosion rate of Steel 3 and vice versa.

The Table shows the results of the corrosion tests at 298 K, while Figs. 1 and 2 show them for 313 and 333 K.

As follows from the obtained data, the corrosion rate of Steel 3 in a 7% NMK solution with no additives or MNZh-5-1 is practically invariant over time. By contrast there is even a small decrease in the

| № опыта TEST | STEEL 3 Ст. 3 K, g/m²·h | z, % | MNZh-5-1 МНЖ-5-1 K, g/m²·h | z, % | Время, ч TIME, h |
|---|---|---|---|---|---|
| 1 | 0,09 | 0 | 0,09 | 0 | 24 |
| | 0,08 | 0 | 0,08 | 0 | 48 |
| | 0,08 | 0 | 0,08 | 0 | 72 |
| | 0,09 | 0 | 0,07 | 0 | 96 |
| | 0,09 | 0 | 0,07 | 0 | 120 |
| 2* | 0,13 | 0 | 0,09 | 0 | 24 |
| | 0,16 | 0 | 0,08 | 0 | 72 |
| | 0,16 | 0 | 0,09 | 0 | 96 |
| | 0,16 | 0 | 0,09 | 0 | 120 |
| 3 | 0,07 | 47 | 0,17 | −94 | 24 |
| | 0,10 | 26 | 0,16 | −91 | 48 |
| | 0,11 | 29 | 0,12 | −64 | 72 |
| | 0,11 | 29 | 0,14 | −60 | 96 |
| | 0,15 | 8,5 | 0,08 | −9 | 120 |
| 4 | 0,17 | −29 | 0,03 | 66 | 24 |
| | 0,15 | −10 | 0,02 | 87 | 48 |
| | 0,13 | 3 | 0,02 | 83 | 72 |
| | — | — | — | — | 96 |
| | 0,11 | 32 | 0,03 | 63 | 120 |
| 5 | 0,12 | 9 | 0,02 | 88 | 24 |
| | 0,11 | 19 | 0,02 | 87 | 48 |
| | 0,01 | 95 | 0,02 | 83 | 72 |
| | — | — | — | — | 96 |
| | 0,06 | 63 | 0,02 | 76 | 120 |
| 6 | 0,02 | 80 | 0,01 | 89 | 24 |
| | 0,02 | 80 | 0,01 | 88 | 48 |
| | 0,03 | 79 | 0,01 | 86 | 72 |
| | 0,03 | 79 | 0,01 | 92 | 96 |
| | 0,03 | 80 | 0,02 | 78 | 120 |
| 7 | 0,02 | 83 | 0,005 | 94 | 24 |
| | 0,02 | 76 | 0,006 | 93 | 48 |
| | 0,04 | 76 | 0,009 | 90 | 72 |
| | 0,03 | 78 | 0,009 | 90 | 96 |
| | 0,03 | 80 | 0,007 | 92 | 120 |
| 8 | 0,02 | 86 | 0,05 | 94 | 24 |
| | 0,02 | 86 | — | — | 48 |
| | 0,03 | 81 | 0,008 | 90 | 72 |
| | 0,03 | 78 | 0,009 | 90 | 96 |
| | 0,03 | 79 | 0,009 | 90 | 120 |
| 9 | 0,02 | 84 | 0,01 | 92 | 24 |
| | 0,02 | 86 | — | — | 48 |
| | 0,03 | 80 | 0,01 | 87 | 72 |
| | 0,03 | 78 | 0,01 | 90 | 96 |
| | 0,03 | 80 | 0,01 | 86 | 120 |
| 10 | 0,14 | 87 | 0,01 | 91 | 24 |
| | 0,06 | 60 | — | — | 48 |
| | 0,06 | 64 | 0,009 | 90 | 72 |
| | 0,06 | 64 | 0,01 | 90 | 96 |
| | 0,04 | 73 | 0,01 | 89 | 120 |

*Steel 3 and MNZh-5-1 are present together

corrosion rate of the MNZh-5-1 alloy in the same situation, which agrees with the earlier work [5]. The test were conducted under static conditions without stirring of the acid solution. The Steel 3 and MNZh-5-1 corrosion rates were found by averaging five parallel tests, as is instructed in the CEMA 4815-84 standard.

When Steel 3 and MNZh-5-1 are both present, the corrosion process changes. First of all, the MNZh-5-1 corrosion rate "stabilizes" at a higher level, and secondly, there is observed a substantial increase in the Steel 3 corrosion rate (by a factor of 1.6 to 2). In addition, there is a significant amount of reduced copper noted on the steel plates, which is difficult to remove by mechanical means.

Introducing thiourea into the NMK solution turns out to have a differing effect on the corrosion process depending on its concentration. For a thiourea concentration of 1 g/dm$^3$ the degree of protection for Steel 3 (the decrease in the corrosion rate) fluctuates between 47 and 8.5% by the end of the experiment, while the degree of protection is chiefly negative relative to MNZh-5-1, i.e. there is an increase by a factor of 1.6 to 1.9 in the corrosion rate. The most beneficial thiourea concentration in this instance should be recognized at 0.25 g/dm$^3$ (test 10, Table), for in this instance the Steel 3 corrosion rate was considerably reduced. Nevertheless we need to point out that in all the tests using thiourea (tests 3 – 5, Table) there was significant precipitation of elementary sulfur and, in addition, to some degree or another all the steel plates had reduced copper deposits on them. The effectiveness of chemical cleaning is reduced when precipitate falls into the recessed areas of the loop, and the presence of cupric deposits on the steel surfaces leads to an increase in the corrosion rate of the loop as a whole and to the need for mechanical cleaning or other measures.

The best idea, as we have proposed, is to apply a reliable protective inhibitor to the entire loop to be cleaned[2]. It was earlier shown[2,6] that a number of the inhibitors we synthesized effectively protect against oxidic corrosion in ferrous metals as well as in the MNZh-5-1 alloy. For reduced corrosion rates in the most highly stressed sections of the loop in chemical cleaning of the heat exchanger, it is relevant to study the inhibitory process when both Steel 3 and MNZh-5-1 are present in the NMK solution.

The addition of 0.5 g/dm$^3$ of some inhibitor gets us from a 78 to a 86% degree of protection for Steel 3 (Table, tests 6 – 9) and from 83 to 94% for MNZh-5-1 alloy. The inhibiting effect for higher concentrations of these compounds is to be found in [1]. We should note that there is a complete absence of reduced copper on the steel samples, consequently the electrochemical process of reducing copper has been completely suppressed.

Negligible concentrations of thiourea lower somewhat the corrosion rate of Steel 3 in the 7% NMK solution.

In order to study possible synergy, a separate series of NMK solutions were prepared that had thiourea and oxidic corrosion inhibitors added at the same time. As was demonstrated in the investigation (Table, test 10), in spite of the absence of reduced copper on the steel plates, the degree of protection of the control samples did not increase, i.e. no synergy was discovered (no increase in the inhibitory effect).

In order to study the effect of cleaning solution temperature on the corrosion process, we also performed tests at the higher temperatures of 313 K and 333 K, which are sometimes employed when acid cleaning carbonaceous deposits. As follows from the data (Fig. 1, 2), the nature of the corrosion process changes almost not at all with increasing cleaning solution temperature in this case, i.e. the presence of thiourea facilitates increased corrosion wear in MNZh-5-1 alloy.

Thus we have studied the effect of both Steel 3 and MNZh-5-1 being present in an NMK solution on the corrosion process. We have remarked on the role of protective screens in chemical cleaning of carbonaceous deposits from heat exchangers. The ineffectiveness of using thiourea under actual circumstances has been recognized. The effectiveness of using a reliable protective inhibitor has been confirmed.

**Bibliography**


1. Berezkin N.N., Kirilyuk S.S., Mindyuk A.K., "Protection of MNZh-5-1 Alloy and Steel in Aqueous Solutions of MNK and Hydrochloric Acid Using Certain Inhibitors in the Acid Cleaning of TES and AES Turbine Condensers", FIZIKO-KHIMICHESKAYA MEKHANIKA MATERIALOV, No 5, 1986

2. Berezkin N.N., Kirilyuk S.S., Isayev N.I. "Inhibitor Protection of the Loop During Chemical Cleaning of Heat Exchanger Equipment", ENERGETIK, No 6, 1987

3. "Khimicheskiye ochistki teploobmennogo oborudovaniya" [Chemical Cleaning of Heat Exchanger Equipment], No 2, ed. by T.Kh. Margulova, Moscow, Energiya, 1978

4. Antropov L.I., Makushin Ye.M., Panasenko V.F. "Ingibitory kislotnoy korrozii" [Acidic Corrosion Inhibitors], Kiev, Tekhnika, 1981

5. Lazarenko Yu.I., Shimanskiy B.A. "Corrosion of Condenser Tubes in Coolant Water After Acid Cleaning", ELEKTRICHESKIYE STANTSII, No 8, 1979

6. Berezkin N.N., Kirilyuk S.S., Dzhigerey O.G., Dovgal Yu.I. "Use of Inhibitors to Lower Frothing During Dissolving of Carbonaceous Deposits in Hydrochloric Acid", ELEKTRICHESKIYE STANTSII, No 5, 1987

UDC [621.311.25:621.039].001.572

**KIPR Time-Dependent Software Package for Investigating the Dynamics of VVER-1000-Equipped AES**

907F0210B Moscow ELEKTRICHESKIYE STANTSII in Russian, No 2, Feb 90, pp 16-20

[Article by I.M. Arshavskiy, C.Tech.S, V.M Dmitriyev, D.Tech.S., S.B. Korolev, engineer, and A.Ye. Kroshilin, D.Tech.S.; VNIIAES]

[Text] A great many studies have been devoted to investigating the thermal and hydraulic processes going on in non-stationary and emergency modes of operation of VVER-1000-equipped AES. Most of the mathematical models and programs that have been developed are directed toward reaffirming the operating safety of the power generating units.

The problems that arise during power generator operation place particular demands on a mathematical model. We will list a few of these.

1. We need to have a mathematical model of the power generating unit as a whole, including the primary process systems, automatic regulators and measuring devices.

2. The mathematical model should be able to be readapted for each different actual AES power generating unit (taking into account the individual technical implementations, adjustments to the automatic regulating systems, etc.), as well be able to process output data for monitoring by AES technologists.

3. The mathematical model should be both fast and accurate.

Satisfying the latter requirement is accomplished by developing a set of mathematical models, each of which has its limited area of application while ensuring efficiency and accuracy. The combination of mathematical models allows us to have a wide range of applicability of the mathematical model as a whole while maintaining its speed.

The complex of computer programs that we have developed were designed on the modular principle. All the AES process equipment and physical processes were nominally divided into groups, each of which was described by a separate functional module (subprogram). Most of the functional models had variant implementations differing in their detail and accuracy of describing the corresponding object or process and, as a result, the computational characteristics of the program: its speed and the amount of computer memory needed. The software package included the following functional modules:

*N* – a subprogram for neutron physics calculations; *H* – a subprogram for modeling the thermal and hydrodynamic properties of the coolant in the primary loop of the AES; *TEPL* – a model describing the temperature fields in the fuel elements, reactor shell and piping; *TPS* – joining the models of the primary

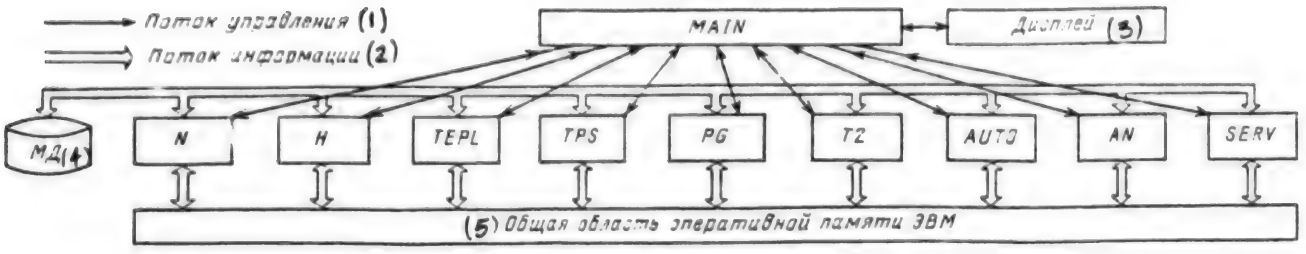


**Figure 1. Structural Diagram of the KIPR Software Complex.** Key: 1 – Control; 2 – Data; 3 – Display; 4 – Magnetic Disk; 5 – Common Area in Computer Main Memory

loop process system and reactor core emergency cooling system, including the pumps for emergency reactor flooding and aftercooling; *PG* – a model of the steam generators and steam lines; *T2* – a model of the secondary loop thermal equipment, including the turbine, condenser, deaerator, steam superheater, etc.; and *AUTO* – a functional subprogram for joining all automatic regulating systems of the primary and secondary loops of the power generating unit. The operation of the automatic systems is described using the real control laws implemented by actual regulators, their adjustment parameters, dead zones, servomotor inertia, etc. *AN* is the model of the AES power system.

To ensure operation of all the program modules in the context of the overall mathematical model, we standardized the content and form of data exchange between program modules, and the rules governing their operation. All data exchanged between the functional modules is located in a common area of the computer's main memory. A dedicated subprogram monitor controls the operation of the functional modules, which organizes calculation of the initial steady-state conditions of the power generating unit and calls the functional modules in cyclic order (modeling a process that is non-steady with respect to time). The monitor also provides interactive operation with the model, so that the researcher has the opportunity to output the model's results in graphic and text form to any number of displays and vary the operating mode of the program in an interactive manner. In addition to the functional modules and control subprogram as a part of the software package, there are also a number of service programs, including *INIT* – a module that accompanies the initial data needed by the software package. Initial data includes several thousand numbers, listed in tables, laden with comments and special indicators. The *INIT* service program substantially simplifies the preparation of initial data for calculations and allows us to construct a mathematical model for an actual power generating unit.

The structure of control and data transfer of the software package is shown in Fig. 1.

This organization of the software complex has the following important advantages permitting efficient use of this tool for operational tasks:

- it enables us to broaden the content and, consequently, to increase the detail and accuracy of the model;
- it gives us flexibility in the modeling system (more accurate, slower models used only in certain circumstances, or, for the majority of calculations, faster and simpler models);
- there are the service programs that allow AES technologists to readjust the mathematical model for actual power generating units and process the output data (including interactively).

We will now give a more detailed description of the fundamental functional modules of the software package. The calculational complex consists of 4 interchangeable versions of a model of the thermal and hydrodynamic state of the coolant in the primary loop of a power generating unit (*H1* – *H4*).

1. The primary job of functional module *H1* is to model the processes associated with large-scale flows in the primary loop of the power generating unit (including the Maximum Design Accident). What is being determined in this case is the correct description of the effect of pressure wave propagation.

One-dimensional time-dependent control of the conservation of mass, momentum and energy in a homogeneous steam-water flow is integrated in. It uses the calculational method of [1], which is a generalization of the Godunov numerical scheme[2] for the case of more complex (as compared to an ideal gas, for which the Godunov method is traditionally employed) control of the state of the steam-water mixture.

We note the advantages of the numerical scheme *H1* is based on as compared to other schemes for hydrodynamic calculations (e.g., the Lax-Vendroff scheme, or the method of characteristics): the *H1* numerical scheme describes more accurately the wave flow of coolant for a minimal number of differencing steps; conservation of mass and energy is built in to the numerical scheme, which is especially important for investigating loss-of-seal in a loop; and the numerical scheme is highly effective and stable for supersonic flows as well as those approaching sound speed.

2. The primary job of model *H2* is also a description of the processes associated with loss-of-seal in the primary loop. A one-velocity two-temperature model of coolant flow is employed. It is assumed that the temperature of the steam is identical to the saturation temperature and it considers only the most significant effect – the possibility of water making the transition to a superheated state in the initial stages of boiling.

The kinetic equations for steam generation include a function for the steam generation intensity, which follows from a generalization of the large amounts of experimental data. It considers boiling at the walls of the tubing as well as within the volume of the superheated liquid on solid impurities.

Article [3] presents the calculational model on which functional module *H2* is based in more detail.

3. When modeling time-dependent AES operating modes with characteristic times on the order of tens of seconds, use of mathematical models *H1* and *H2* is involves significant outlays of machine time. This is in connection with the Curant limit $\Delta t \leq \Delta x / | v \pm c |$, which determines when to "compress" the propagation of acoustic disturbances.

We may point out that there is a rather broad class of slow time-dependent modes in which wave effects are not decisive and use of mathematical models *H1* and *H2* is not justified.

Mathematical model *H3* is based on a quasi-stationary calculation method for the coolant flow in the loops of a power plant [4]. This method describes the quasi-stationary flow class in which variations in velocity and pressure over time are governed primarily by the time-dependent boundary conditions and variations in the external parameters. Nondimensional analysis shows that an integrated, simplified system of hydrodynamic equations is accurate enough for this class of flows: time-independent equations for velocity $v$ and pressure $p$, and time-dependent equations for the density $\rho$. The Curant stability condition for this case has the form $\Delta t \leq \Delta x / | v |$, which enables us to construct solutions with larger time steps.

For description of the effects of boiling and condensation caused by pressure changes over time, we use a constant-volume idealization, appropriate to which we introduce the unknown parameter $dp^*/dt$, which characterizes the speed of pressure changes over the loop.

For integrating the continuity equations we use a conservative numerical scheme [5] based on analytical solution of the decay of an arbitrary density discontinuity in a two-phase two-velocity steam-water flow. The fundamental steam-water flow regimes are considered: bubble, slug, eddy, disperse, and transitional regimes.

Thus functional module *H3* ensures conservation of mass and energy, takes into account the expansion of coolant because of changes in pressure over time, and correctly describes the effects of velocity nonuniformity with a small number of calculation steps.

4. In the modeling, a fairly broad class of nonstationary AES modes do not require a high degree of accuracy in descriptions of the coolant flow in the primary loop of the power generating unit. The slow, nonstationary processes with characteristic times from hundreds to thousands of seconds in which the coolant remains one-phase are an example of this.

We have developed a simplified hydrodynamics mathematical model *H4* for description of these regimes, and for performing multivariate quantitative calculations.

The primary loop of a power generating unit is represented by three elements (the mixing chambers and the pressurizer) with averaged parameters. Changes in the flowrate of coolant over the length of a loop and core channels are ignored, and we also do not take into account the time it takes for coolant to pass through the loops and core channels. The key to the method is the following assertion:

$$dp_{NKS}/dt = dp_{VKS}/dt. \tag{1}$$

From the equations of conservation of mass and energy, we obtain a relation for the rate of change in the pressure in the NKS and VKS [not further identified] with respect to time.

The total system of equations for determining the pressure and flowrate in the loop includes equations of the form $\Delta p = \xi G^2$ (where $\xi$ is a known coefficient) for the loop and core channels, the equation of conservation of energy for the pressurizer, and balancing equations of conservation of energy for the loop as a whole. We propose an implicit calculation scheme for solving these equations, which allows us to increase the time integration step up to 1 s. This makes the functional model quite fast. In additional, mathematical model *H4* provides enough accuracy for engineering calculations, which follows from a comparative analysis of its operation, experimental data, and calculations from the models *H3* and *H1*.

The software package includes two interchangeable models for neutron physics processes in the reactor core (Nos 1 and 2).

1. This model is designed to describe the processes in which spatial neutron physics effects are insignificant. Mathematical model No 1 is based on integrating the equations of point kinetics in a quasi-stationary approximation with delayed neutrons being broken down into six different groups. It also considers fast feedback on fuel temperature, water temperature and boron concentration. For a calculation of the reactivity induced by the control rods we use an experimental dependence of the integral effectiveness of a control rod bundle as a function of the depth of penetration into the core.

2. Module No 2 is designed for a description of the spatial distribution of the neutron flux in the core. The core is divided into 10 calculation regions, and in each of these the neutron flux is considered to be piecewise-continuous. A quasi-stationary one-velocity diffusion approximation is used, with delayed neutrons being broken down into six different groups.

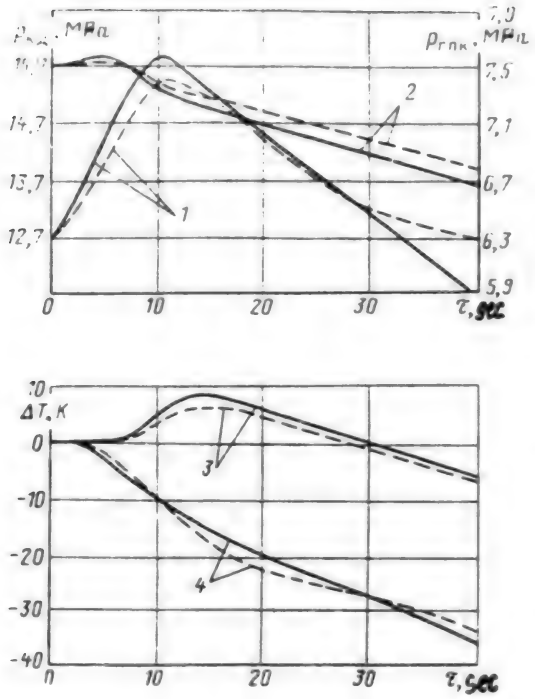


**Figure 2. Graph of Pressure in the Second Loop (*1*) and in the First Loop (*2*), and Variations in Temperature at the Reactor Inlet (*3*) and Outlet (*4*) as a Function of Time in the Closed SRK Turbine Mode (With Triggering of the Emergency Shutoff):**
———— – DINAMIKA program calculations;
– – – – – – KIPR program calculations

medium is represented in the form of a piecewise-continuous function that is independent of the spatial coordinates at the boundaries of each of the calculational regions).

The very real advantage of this model is its efficiency, which makes it possible to use neutron kinetics model No 2 for multivariate calculations.

A mathematical model of the horizontal steam generator has been developed in two interchangeable variants (functional modules *PG1* and *PG2*), differing in the detail in their description of thermal and hydrodynamic processes, which are realized in steam generators in the time-dependent operating

For integration of the neutron kinetics equations we use a method based on expansion of the neutron flux density function in terms of eignenfunctions of the Laplace operator, which allows us to reduce the problem of integrating the initial differential equations to solution of a system of linear algebraic equations in terms of the average neutron flux over the core (here the breeding characteristic curve of the

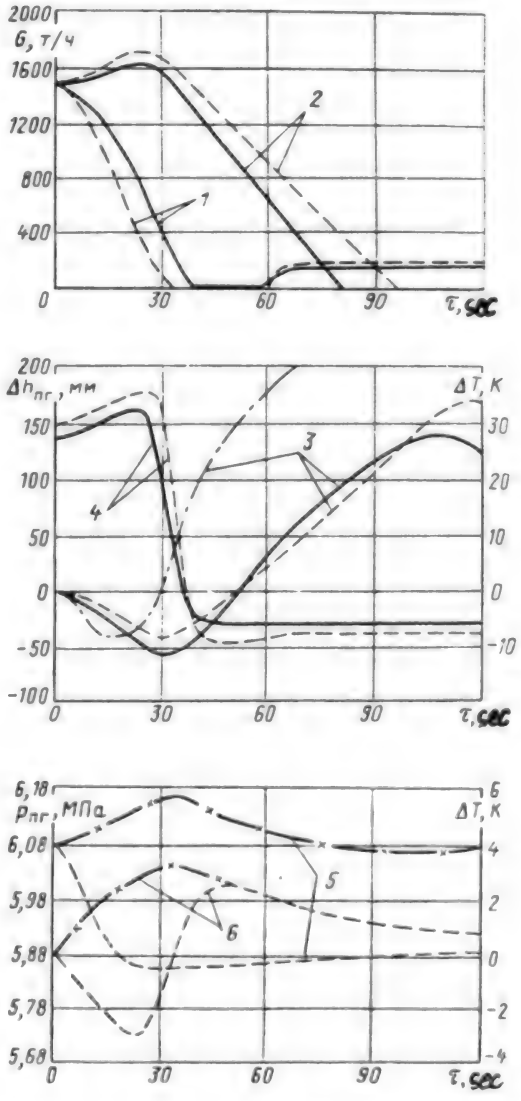


**Figure 3. Graph of Variation in Parameters for Switching Off One of the Main Circulating Pumps at YuUAES:** 1 – Flowrate of steam from the "emergency" steam generator; 2 – Flowrate of feedwater into it; 3 – Level in the steam generator with respect to a baseline of 1000 mm; 4 – difference in temperature between the hot side and cold side; 5 – pressure in the steam generators; 6 – pressure in the hot side: ———— – experiment, – – – – – calculation for the "emergency" loop, —x—x—x— calculation for the "non-emergency" loop, —·—·—·— level readings without consideration of inertia

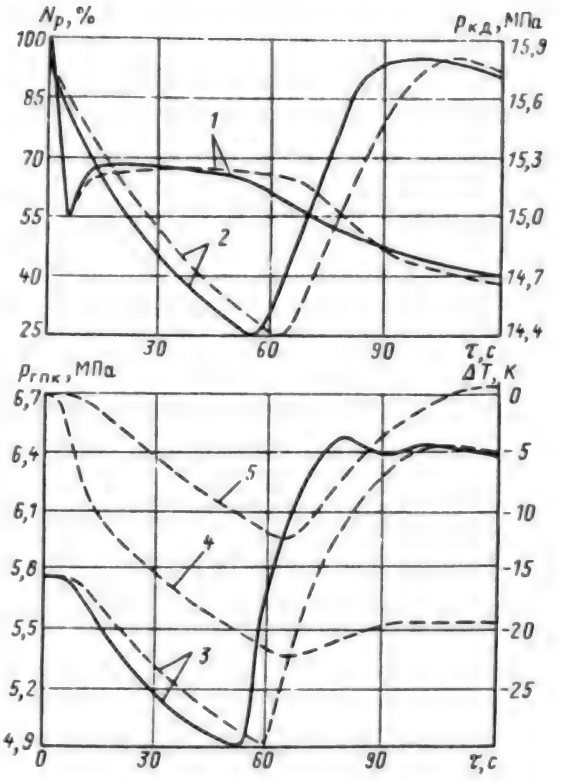


**Figure 3. Graph of Variation in Parameters for a False Triggering of the Scram System at the KaAES:**
1 — Neutron power; 2 and 3 — Pressure in KD and GPK; 4 and 5 — temperature at the reactor inlet and outlet, ——— — experimental, — — — — — calculation

regimes of a power generating unit. Both models (*PG1* and *PG2*) include a description of the steam generators and steam lines connecting them to the turbines. We introduce a description of the more complicated model *PG2*.

In modeling of steam generators, the most complex problem is determining the water level. The *PG2* distributed model was developed for a detailed description of the processes in the two-phase volume of the steam generator. It takes into account the following primary effects that substantially influence the thermal and hydraulic state of the steam generator and the water level readings in time-dependent processes: phase slipping in the steam-water volume of the steam generator, natural circulation of coolant, variations in pressure drops over the submerged tube plate, the complex geometry of that plate, and the presence of flow at the edges.

The presence of the submerged tube plate and natural circulation of coolant in the steam generator results in a number of instances in the level gauge readings differing substantially from the actual amount of water in the generator. In determining the level gauge readings, model *PG2* calculates the drop in pressure which will be measured by the gauge. The equalizing vessel with pulse lines is also modeled, which enables us to describe the effect of needle inertia in the level readings. This ensures a fairly high degree of accuracy in predicting level readings during time-dependent processes.

The mathematical model for the unit's automatic regulation system is implemented in only one variant. The functional module *AUTO* models the work of the primary AES power generating unit regulation system in normal, transition and emergency modes, corresponding to complete or partial power reductions. The model describes the control system of the primary loop of a reactor, the pressurizer, the secondary loop and turbine. Analysis of the values of controlled and observed variables, realization appropriate to the structure of the regulation and control algorithms, and the formation and transfer of vector control actions to the other subprograms are all functions of the *AUTO* module. The *AUTO* module compares current parameters with set values and generates safety signals or interlock signals, as well as diagnostic information.

The modeling of the regulation system was carried out in volume, allowing us to reproduce the operation of the power generating unit over the range of powers and to realize all normal and emergency modes. Operation of the regulators were described by differential equations appropriate to the regulation guidelines that shape them. Static as well as dynamic regulator parameters were taken into account.

One of the most important stages in the development of each functional module included in the mathematical model software package is comparing the results of its operation with experimental data

and with calculations from more accurate models. This kind of independent testing lets us verify that the approximations made in the mathematical models are fair, and to refine the cross-coefficients in the correlations used.

In order to check on the package as an adequate mathematical model of the object, we conducted a comparison of the calculations and experimental data obtained during dynamic tests in AES. A comparison was also made with the DINAMIKA program[7].

Fig. 2 shows a graph of the changes in unit parameters when the turbine SRK are closed (with triggering of the emergency shutoffs). The graph in Fig. 3 illustrates the calculational and experimental results in which one of the four main circulation pumps that operate under nominal power is switched off, which happened at the YuUAES[6]. The graph in Fig. 4 characterizes the results of the false plunging of the control rod bundle into the core, as conducted at the KaAES No 2 unit.

The good agreement between calculation results and dynamic test data (about 30 different modes were processed in all) opens up the possibility of using the KIPR software package for meeting a wide range of needs arising in the process of operating an AES, including the development of instructional methods for the operating personnel.

**Bibliography**


1. Gofman G.V., Kroshilin A.Ye., Nigmatulin B.I. "Time-Dependent Wave Efflux of Boiling Liquids from Vessels", TVT Vol 19 No 6, 1981

2. Godunov S.K. et al., "Chislennoye issledovaniye mnogomerbykh zadach gazovoy dinamiki" [Numerical Investigation of Multidimensional Problems in Gas Dynamics], Moscow, Nauka, 1976

3. Kozyrev L.I., Kroshilin A.Ye. "Efficient Calculation Method for Wave Efflux of Non-Equilibrium Boiling Steam-Water Flows" in "Gazodinamika mnogofazhykh potokov v energoystanovkakh. Mezhvuzovskiy sbornik nauchnykh trudov" [Gaz Dynamics of Multiphase Flows in Power Plants. InterVUZ Collection of Scientific Articles], Kharkov, 1987

4. Arshavskiy I.M., Klebanov L.A., Kroshilin A.Ye. et al., "A Thermal and Hydraulic Model of Time-Dependent Flows in the KMPTs Power Generating Unit Equipped with the RBMK-1000 Reactor", VOPROSY ATOMNOY NAUKI I TEKHNIKI. SER. FIZIKA I TEKHNIKA YADERNYKH REAKTOROV, No 2, 1986

5. Klebanov L.A., Kroshilin A.Ye., "On the Applicability and Properties of a Model of Slippage in Two-Phase Flows", VOPROSY ATOMNOY NAUKI I TEKHNIKI. SER. FIZIKA I TEKHNIKA YADERNYKH REAKTOROV, No 2, 1985

6. Pavlysh O.N., Garbuzov I.P., Reukov Yu.N., et al., "Experimental Verification of the Qulaity of Automatic Regulation of Supply to Steam Generators for a VVER-1000-Equipped Power Generating Unit Using a Variety of Master Signals", ELEKTRICHESKIYE STANTSII, No 5, 1986

7. Spasskov V.P., Volkov G.A., Volkov V.A. et al., "Program for the BESM-6 Computer. Calculation of the Time-Dependent Modes of a VVER-Equipped Power Plant--DINAMIKA. 1776/OFAP, 1978", TsNIIATOMINFORM, No 3-4, 1979

UDC 621.165.004.67

**On the Operational Reliability of the LMZ VK-100-90 Turbine**

907F0210C Moscow ELEKTRICHESKIYE STANTSII in Russian, No 2, Feb 90, pp 27-30

[Article by Yu.M. Gofman, C.Tech.S., Sverdlovenergoremont]

[Text] VK-100-90 turbines operate at $p = 90$ kgf/cm$^2$, $T = 500$°C and at present have logged about 300,000 h.

In accordance with the technical reequipment plan of USSR Minenergo, all condenser turbines of this brand are to be written off, and turbines converted over to central-heating uses will be modernized, in which the replacement of the high-pressure cylinder in the assembly is stipulated.

This article presents material about inspection of the metal in the turbine as a whole, in both the high-pressure and low-pressure cylinders.

**High-Pressure Cylinder Housing.** By inspecting the condition of the metal in this turbine after 200,000 h of operation, we have shown that the high-pressure cylinder may be operated reliably for up to 500,000 h[1,2]. This conclusion was drawn on the basis of defectoscope monitoring, studies of microstructure zones over the operating temperature regimes of the turbine, analysis of the fine structure, and study of the phase analysis and mechanical properties.

Recently we conducted additional studies with estimates of the crack resistance of 20KhML steel and investigation of the condition of the turbine metal after 275,000 h. As is known, the cyclic ultimate strength and crack resistance criteria should be numbered along with the static and long-term strength as limiting criteria of the condition of the turbine housing.

The primary method for estimating the crack resistance in the process of operating the turbine is magnetic powder defectoscopy (MPD) at the radius transitions. After 300,000 h of operation the housing parts were subjected to monitoring three and four times. Thirteen turbines were subjected to this monitoring, installed in three different electric power stations. The turbines operated in a base-load regime. The operating period of all the turbines was practically identical. The number of starts ranged from 200 to 500.

Table 1 presents the data on the number of detected cracks, and Table 2 gives the depth characteristics of the cracks.

All the cracks occurred only on exterior surfaces.

Table 1

| Control object | Number of cracks over the operating period, in thousand of hours | | | |
|---|---|---|---|---|
| | up to 100 | 100 – 150 | 150 – 200 | 200 – 250 |
| HPC Housing | 5 | 6 | 41 | 35 |
| HPC Cover | 21 | 20 | 20 | 18 |
| Stop Valve | 6 | 2 | 13 | 11 |
| Regulator Valve | 19 | 18 | 25 | 13 |

Table 2

| Control Object | Crack Depth, in mm | Number of cracks over the operating period, in thousands of hours | | | |
|---|---|---|---|---|---|
| | | up to 100 | 100 – 150 | 150 – 200 | 200 – 250 |
| HPC Housing | up to 5 | – | 4 | 5 | 23 |
| HPC Cover | | – | 12 | 3 | 7 |
| Stop Valve | | – | – | 1 | – |
| Regulator Valve | | – | 9 | 2 | 7 |
| Housing | 5 – 15 | 1 | 11 | 16 | 12 |
| Cover | | 18 | 8 | 11 | 6 |
| Stop Valve | | 4 | 1 | 4 | 3 |
| Regulator Valve | | 12 | 4 | 20 | 9 |
| Housing | 15 – 30 | – | 1 | 7 | 4 |
| Cover | | 2 | – | 4 | 1 |
| Stop Valve | | – | – | 5 | 6 |
| Regulator Valve | | 1 | – | 3 | – |
| Housing | 30 | – | – | 6 | 4 |
| Cover | | – | – | – | 3 |
| Stop Valve | | 2 | 1 | 3 | 1 |
| Regulator Valve | | 3 | 1 | 1 | 1 |

An investigation of the cracks in the high-temperature region of the housing showed that the cracks are characteristic of heat-fatigue, are filled with oxides, and have pinched, dead ends (Fig. 1). This character of the cracks testifies to their thermal origin.

We should note that the damage in each of the power stations is not identical. Thus at one power station there are practically no defects at all on cast parts, while conversely at another there are defects on practically all the cast parts.

The most damaged area of the housing is the exterior surface of the chamber of the regulator stage.

In recent years VTI and TsKTI have developed a method for determining the crack resistance of the metal in cast turbine housing parts[3,4]. The crack resistance characteristics were determined by this method for the metal of three turbine housings after 200,000 h of operation.

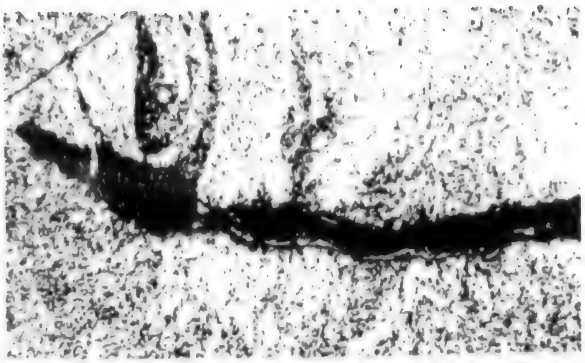

Рис. 1

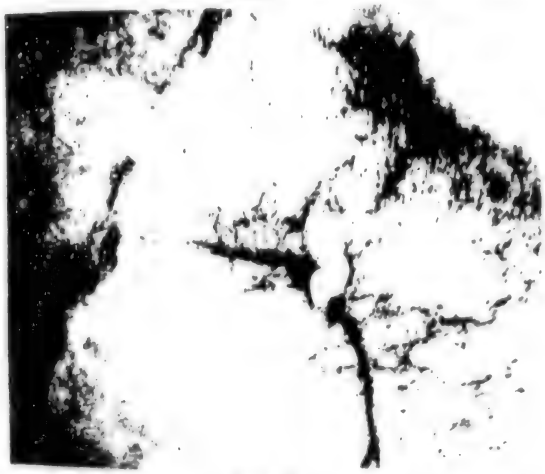

Рис. 2

Рис. 3

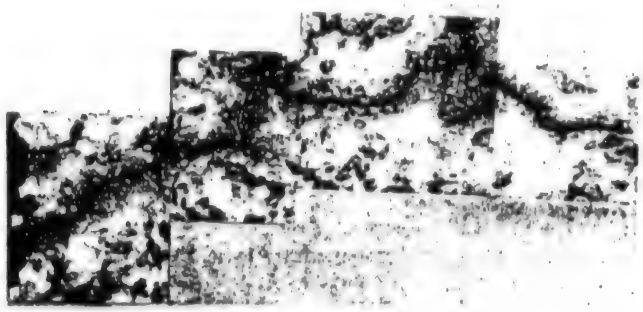

Рис. 4

Рис. 5

Рис. 6

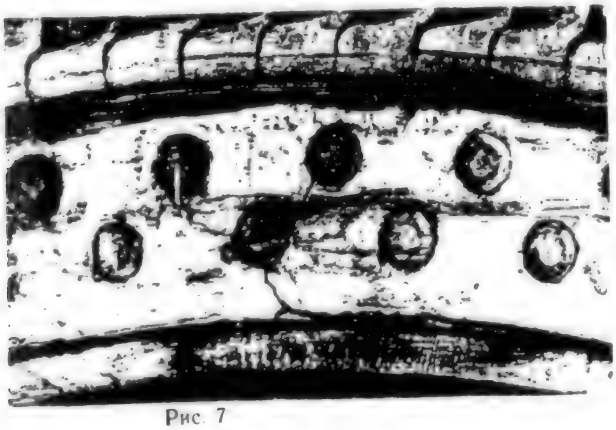

Рис. 7

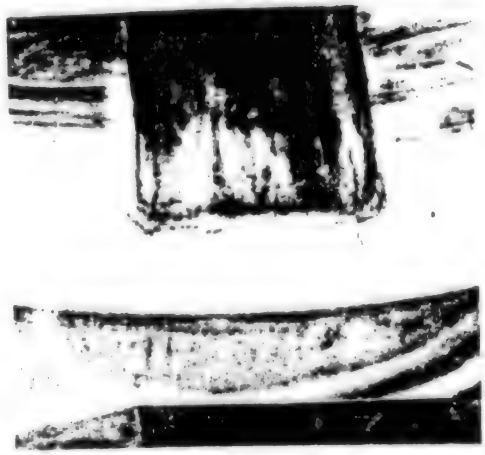

Рис. 8

The mechanical properties estimated from standard samples are given below (1 is for no cracks over the entire period of operation, 2 is for an average number of defects – 12, and 3 is the maximum number of crack formations observed over all the 13 turbines – 25).

| | 1 | 2 | 3 | PMTU-17-56 (LMZ) |
|---|---|---|---|---|
| $\sigma_B$, MPa | 470.0 | 440.0 | 485.0 | 470.0 |
| $\sigma_C$, MPa | 314.0 | 300.0 | 268.0 | 250.0 |
| $\delta$, % | 26.0 | 26.0 | 26.0 | 18.0 |
| $\psi$, % | 59.0 | 51.0 | 59.0 | 30.0 |
| $a_K$, kJ/m$^2$ | 700 | 98 | 147 | 290 |
| $H_B$ | 170 | 143 | 149 | 135 – 180 |

The hot hardness $H_B$ and critical coverage $\sigma_K$ determined by the VTI method, and the critical coverage $\sigma_C$ determined by the TsKTI method are presented below.

| | $H_B$ | $\sigma_K$, mm | $\sigma_C$ |
|---|---|---|---|
| 1 | 1200 | 0.25 | 0.25 |
| 2 | 1000 | 0.40 | 0.20 |
| 3 | 1100 | 0.35 | 0.22 |

From an examination of this data it follows that the crack-resistance characteristics for 20KhML steel in all cases exhibit satisfactory values.

A study of the metal after 275,000 h of operation at the recommended capacity shows that the metal is in satisfactory condition[5]. In addition to the accepted methods, the high-pressure cylinder metal was subjected to an evaluation of damage in terms of the criteria proposed in [6,7]. The damage was determined from electron microscope investigation of foils, electron fractography of low-temperature breaks, and optical metallography. Viewing a large number of foil sections revealed that damage to the metal was low, and only a small number of individual micropores 0.1 – 0.3 $\mu$m in size were detected along the boundaries of the ferrite grains (Fig. 2).

We should note that damage to the metal as estimated from the dislocation structure of ferrite was not taken into consideration, since the metal has a large-grain structure and there is practically no separation of carbides by the main part of a grain. Thus fragmentation and formation of cell-like structures were noted in the metal.

Investigation reveals that the breaks are brittle and mixed, encountering both transcrystalline sections and sections of between-grain breaks. Only a few fine pores were found by examining the breaks on a scanning microscope, which established that the grain boundaries are hardly damaged at all (Fig. 3).

Metallographic analysis on an optical microscope detected no pores.

Thus this investigation of housing parts has shown that in terms of all the indicators – crack effects, crack resistance, microstructural conditions, mechanical properties, phase composition and carbide formation processes, in terms of damage the metal is in satisfactory condition.

**High-Pressure Rotor.** Now we will conduct a fairly detailed investigation of the struc ural condition of the metal in the rotor after extended operation[8], which revealed an absence of substantial alteration in the structure and properties. We followed the condition of a large number of high-pressure rotors using non-destructive monitoring methods. Practically all the checked rotors were free of defects. Defects were detected in all on only a few rotors. Investigation of the nature of the defects showed that these cracks were metallurgical in origin and located near segregated material; long-term operation does not lead to them opening any further.

Fig. 4 presents a typical crack 4 mm deep found in the regulator stage area, which hardly grew at all after 210,000 h of operation. This leads us to the conclusion that the level of active stress in the rotor is substantially less than what has been calculated.

Thus the stability of the properties of 34KhM1A steel during extended operation and the absence of action on the rotor of a cyclic stress nature that would cause crack generation all point to the possibility of further reliable long-term operation of the high-pressure rotor.

**Low-Pressure Housing.** When following the condition of housings after 200,000 h of operation, we no.ed considerable corrosional and erosional wear. Washings were found on the cylinder baffles, washouts of the guidevane roots along the inner generatrix and throat of the diaphragm, washings on the diaphragm joints and at the guidevane roots, and wear of the flow separator (Fig. 5).

**Low-Pressure Rotor.** Washouts were found on the disks along the outside near the rivets on the steam intake side (Fig. 6).

Annular cracks were located on the radius transitions from the circumference to the balance band. Radial cracks were found near the rivet holes (Fig. 7). Cracks were found in the keyways (Fig. 8). There were washouts in the hub of the disk below the diaphragm seals extending to the disk apron.

Thus this data indicates that the operational reliability of the low-pressure cylinder falls off sharply after 200,000 h of operation due to corrosional/erosional wear of the disk, diaphragm, baffles and flow separator, as well as corrosional/fatigue cracking of the disks in 13 to 19 of the stages.

**Conclusions.**

1. The high-pressure cylinder of the VK-100-90 turbine may be reliably operated for up to 500,000 h with vigilant monitoring after cracks begin forming in the disk slots beneath the blades.

2. The low-pressure cylinders are not operationally reliable after 250,000 h of operation, requiring large outlays during capital repairs.

3. Turbines that are to be converted to central-heating uses do not require replacement of the high-pressure cylinder, as has been specified in the program, but rather of the low-pressure cylinder.

## Bibliography

1. Gofman Yu.M., Kasantseva N.S. "Investigation of the Condition of Housing Parts of the K-100-90 Turbine After 200,000 h of Operation" in "Tezisy dokladov na soveshchanii "Sistema kontrolya i otsenka nadezhnosti i dolgovechnosti metall v energoustanovkakh" [Reports to the Conference on "Systems for Monitoring and Evaluating the Reliability and Durability of Metal in Power Plants], Moscow, VDNKh, 1981

2. Gofman Yu.N., Kasantseva N.S. "Reliability of VK-100 Turbine Housing Parts After Long-Term Operation", ELEKTRICHESKIYE STANTSII, No 4, 1984

3. Gladshteyn V.I., Sheshenev M.F. "On Reliability Criteria of Cast Metal Parts in Turbines Made of 15Kh1M1FL", TEPLOENERGETIKA, No 6, 1979

4. "Rukovodyashchiye ukazaniya. Vypusk 44. Metod opredeleniya treshchinostoykosti materialov energooborudovaniya pri vysokikh temperaturakh" [Guidelines. No 44. Method for Determining the Crack Resistance of the Metal in Power Generating Equipment at High Temperatures], Leningrad, TsKTI, 1981

5. "Instruktsiya po kontrolyu za metallov kotlov, turbin i truboprovodov. I 34-70-013-84" [Instructions for Monitoring the Metal in Boilers, Turbines and Tubing], Moscow, Soyuztekhenergo, 1984

6. Gofman Yu.M., Losev L.Ya., Kazantseva N.S., Nevolina G.S. "Methods of Diagnosing the Condition of the Metal in Steam Piping", ENERGETIK, No 10, 1986

7. Gofman Yu.M., Losev L.Ya., "Estimating the Degree of Damage in Metals Operating at Elevated Temperatures Under Stress", MITOM, No 10, 1985

8. Boyko L.M., Novgorodtseva L.B., Filimonova L.Ye. "Structure and Properties of Metal in the Rotor of a K-100-90 Steam Turbine After Long-Term Operation", ELEKTRICHESKIYE STANTSII, No 11, 1984

UDC 539.319

# OPTIMIZING PARAMETERS OF TRANSITION REGION OF FIBER OPTIC LINE UPON SHARP EXTERNAL PRESSURE DROP

907F0282A Tbilisi SOOBSHCHENIYA AKADEMII NAUK GRUZINSKOY SSR in Russian No 2, Nov 1989 (manuscript received 28 Apr 89) pp 313-316

[Article by M. V. Kvimsadze, N. D. Macharadze, M. V. Ninua, and O. N. Chavchadnidze]

[Text] The situation frequently arises in design of optical communication systems when the light guide changes from the high-pressure to the low-pressure zone. A sharp drop of external pressure, acting on the fiber, leads to intermittent variation of its elastic characteristics at the interface of zones, which in turn leads to the corresponding variation of the dielectric constant of the fiber. Therefore, the emission, propagated along the fiber, is reflected at the zone interface. It is physically obvious that energy losses of the information signal, caused by reflection, will be minimal if the pressure drop is smooth and extended on some section of the fiber. It should be noted that smooth variation of the stress tensor components contributes not only to a decrease of radiant energy losses, but also to a decrease of the probability that the fiber will chip on the section of the pressure drop, which is in itself an important problem.

To reduce the pressure jump, a transition region of the fiber from the direction of the high-pressure zone must be covered by protective material, the elastic characteristics and configuration of which should be selected so that the radiant energy losses be minimal.

The distribution of elastic stresses along the fiber on the transition region was studied in this paper and the conditions at which the pressure jump is minimal were determined. Taking the symmetry of the problem into account, let us write the equations of elasticity in a cylindrical coordinate system [1]:

$$2(1-\nu)\frac{\partial}{\partial r}\left[\frac{1}{r}\frac{\partial}{\partial r}(ru_r)\right]+\frac{\partial}{\partial z}\left[\frac{\partial u_z}{\partial r}+(1-2\nu)\frac{\partial u_r}{\partial z}\right]=0,$$

$$(1-2\nu)\frac{1}{r}\frac{\partial}{\partial r}\left(r\frac{\partial u_z}{\partial r}\right)+\frac{\partial}{\partial z}\left[\frac{1}{r}\frac{\partial(ru_r)}{\partial r}+2(1-\nu)\frac{\partial u_z}{\partial z}\right]=0. \quad (1)$$

where $\nu$ is Poisson's coefficient of matter, $u_r$ is the radial displacement of the particle, and $u_z$ is the displacement of the particle along the axis of symmetry of the structure, coinciding with axis z.

Let us discuss the boundary conditions to the equations of elasticity:

a) It is obvious that radial displacements at the fiber-protective material interface are identical for both media:

$$u_{1r}(r_0)=u_{2r}(r_0). \quad (2)$$

Here and further subscript "1" is ascribed to the fiber, while subscript "2" is ascribed to the protective material, and $r_0$ is the radius of the fiber.

b) Assuming that the adhesion between the fiber and protective material is sufficiently good, one can assume that the axial displacements at point $r = r_0$ for both materials are identical:

$$u_{1z}(r_0)=u_{2z}(r_0). \quad (3)$$

c) The radial stresses at the interface $r = r_0$ in the fiber and protective material are identical:

$$\sigma_{1r}(r_0)=\sigma_{2r}(r_0). \quad (4)$$

d) The protective material-external "internal pressure" medium should be set equal at the interface to the external pressure [2]:

$$\sigma_{2mq}n_q=p_m. \quad (5)$$

where $\sigma_{mq}$ are the components of the stress tensor, $n_q$ are the components of the external normal to the surface of the protective layer, and $p_m$ are the components of external pressure.

If the equation of the generatrix of the cone-like protective layer is written in the form of r = r(z), boundary condition (5) will assume the form

$$\sigma_{rr}+p=\sigma_{rz}\frac{dr}{dz}, \qquad (\sigma_{zz}+p)\frac{dr}{dz}=\sigma_{rz}. \tag{6}$$

The following boundary conditions should be added to the conditions of (2)-(4) and (6)

$$u_r(r=0)=0, \quad u_z(z=0)=0. \tag{7}$$

Let us find the solution of system (1) in the following form:

$$u_z=\frac{z^3}{R}f(r)+zF(r), \qquad u_r=\frac{z^2}{R}\varphi(r)+R\Phi(r). \tag{8}$$

Substituting these expressions into equations (1), it is easy to determine the functions contained in formulas (8):

$$\begin{aligned}
f(r)&=c^{(1)}\ln\frac{r}{R}+c^{(2)},\\
\varphi(r)&=c^{(3)}\frac{r}{R}-\frac{3}{4(1-\nu)}c^{(1)}\frac{r}{R}\ln\frac{r}{R}+c^{(4)}\frac{R}{r},\\
F(r)&=-\frac{1}{1-2\nu}\frac{r^2}{R^2}\left[c^{(3)}-\frac{3}{8}\frac{8(1-\nu)^2-1}{1-\nu}c^{(1)}+3(1-\nu)c^{(2)}\right]-\\
&\quad-\frac{3}{4}c^{(1)}\frac{3-2\nu}{(1-\nu)}\frac{r^2}{R^2}\ln\frac{r}{R}+c^{(5)}\ln\frac{r}{R}+c^{(6)},\\
\Phi(r)&=\frac{1}{1-2\nu}\frac{r^3}{8R^3}\left[4\nu c^{(3)}-\frac{3}{4}\frac{5-8\nu}{1-\nu}c^{(1)}+3c^{(2)}\right]+\\
&\quad+\frac{3}{1-\nu}c^{(1)}\frac{r^3}{8R^3}\ln\frac{r}{R}-\frac{c^{(5)}+2(1-2\nu)c^{(4)}}{4(1-\nu)R}\left(r\ln\frac{r}{R}-\frac{r}{2}\right)+\\
&\quad+c^{(7)}\frac{r}{R}+c^{(8)}\frac{R}{r}.
\end{aligned} \tag{9}$$

where $c^{(j)}$ $(i=1, 2, j=1, 2...8)$ are the desired constants, determined from the boundary conditions, and R is the cross-sectional radius of the protective layer at z = 0.

Let us further consider cases when Poisson's coefficients of the fiber and protective layer are identical ($\nu_1 = \nu_2 = \nu$). Having used the known formulas (see [2] for example) that link $\sigma_{mq}$ to the components of the particle displacement vector and substituting formulas (8) and (9) into boundary conditions (2)-(4), (7), and (8), we find the following relations for the desired constants:

$$
\begin{gathered}
c_1^{(1)}=c_2^{(1)}=c_1^{(5)}=c_2^{(5)}=c_1^{(4)}=c_1^{(8)}=0, \quad c_1^{(2)}=c_2^{(2)}, \\
c_1^{(3)}=c_2^{(3)}+\frac{R^2}{r_0^2}\,\beta\,(c_2^{(3)}+3\nu c_2^{(2)}), \quad c_2^{(4)}=\beta\,(c_2^{(3)}+3\nu c_2^{(2)}), \\
c_1^{(6)}=c_2^{(6)}+\frac{\beta}{1-2\nu}\,(c_2^{(3)}+3\nu c_2^{(2)}), \\
c_2^{(8)}=\beta\left[c_2^{(7)}+\nu c_2^{(6)}+\frac{r_0^2}{8R^2}\,(4\nu c_2^{(3)}+(3-4\nu)\,3c_2^{(2)})\right]+ \\
+\frac{\beta c_2^{(4)}}{E_2-E_1}\left[-E_1\,\frac{\nu(1-\nu)}{1-2\nu}+\frac{1-2\nu}{2(1-\nu)}\,E_1\left(\ln\frac{r_0}{R}-\frac{1}{2}\right)-\right. \\
\left.-E_2\,\frac{1-2\nu}{2(1-\nu)}\left(\ln\frac{r_0}{R}+\frac{1}{2}-\nu\right)\right], \\
c_1^{(7)}=c_2^{(7)}+\frac{R^2}{r_0^2}\,c_2^{(8)}-\frac{\nu}{2(1-2\nu)}\,c_2^{(4)}-\frac{1-2\nu}{2(1-\nu)}\,c_2^{(4)}\left(\ln\frac{r_0}{R}-\frac{1}{2}\right)
\end{gathered}
\tag{10}
$$

where the following notation is introduced

$$
\beta=\frac{r_0^2}{R^2}\,\frac{E_2-E_1}{E_1+E_2(1-2\nu)}, \tag{11}
$$

$E_1$ and $E_2$ are Young's modulus of the fiber and protective material, respectively.

It now remains to use boundary conditions (6). It follows from general analysis of conditions (6) that a significant reduction of pressure on the fiber at $z \to 0$ may occur only with a slow decrease of function $r(z)$. One can also establish that conditions (6) in the region of $z \simeq R$ are fulfilled for any $z$, if $r(z)$ has the form

$$
r=R\exp\left(-\alpha\,\frac{z^2}{R^2}\right). \tag{12}
$$

The dimensionless parameter $\alpha$ in this expression determines the rate of decrease of the generatrix of the cone-line protective layer and, as follows from the above arguments, should satisfy the inequality

$$\alpha \ll 1. \tag{13}$$

Substituting (12) into boundary conditions (6) and taking into account relations (10), one can calculate the constants $C^{(j)}_i$, and one can then use them to calculate the distribution along the coordinates of the stress tensor components in the fiber. They have the following form:

$$\sigma_{1rr}=\sigma_{1\varphi\varphi}=-p\,\frac{E_1}{E_1+(1-2\nu)E_2}\,\frac{1}{1-(1-2\nu)\beta}\left[1+\frac{2\alpha(1-2\nu)\beta}{1-(1-2\nu)\beta}\,\frac{z^2}{R^2}\right],$$

$$\sigma_{1zz}=-p\,\frac{E_1}{E_2}\,\frac{1}{1-(1-2\nu)\beta}\left\{1+2\nu\,\frac{R^2}{r_0^2}\beta+\right. \tag{14}$$

$$\left.+\frac{2\alpha(1-2\nu)\beta^2}{1-(1-2\nu)\beta}\left[2\nu\left(1+\frac{R^2}{r_0^2}\right)-1\right]\frac{z^2}{R^2}\right\}.$$

Terms proportional to $\frac{r^2}{R^2}$ were not considered in derivation of formulas (14), since, besides small parameter $\alpha$, they contain small numerical coefficients.

Analysis of formulas (14) shows that a significant decrease of pressure at z - 0 occurs only if the parameters of the protective layer R, $\nu$ and $E_2$ satisfy the inequality

$$\frac{E_2}{E_1}\gg\frac{2(1-\nu)}{(1-2\nu)\left(1-\frac{r_0^2}{R^2}\right)}. \tag{15}$$

Thus, to reduce the energy losses of the information signal passing through the optical system with the section of the pressure drop, it is necessary that the parameters of the transition region satisfy conditions (13) and (15).

BIBLIOGRAPHY


1. Muradyan, A. G., I. S. Goldfarb and V. P. Inozemtsev, "Opticheskiye kabeli mnogokanalnykh liniy svyazi" [Optical Cables of Multichannel Communication Lines], Moscow, 1987.

2. Landau, L. and Ye. Lifshits, "Teoriya uprugosti" [Elasticity Theory], Moscow, 1965.


- END -

# END OF FICHE DATE FILMED

16 July 1990